nature neuroscience

Sharp wave ripples during learning stabilize the hippocampal spatial map

Lisa Roux[1], Bo Hu[1,5], Ronny Eichler[1,5], Eran Stark[1,2] & György Buzsáki[1,3,4]

Cognitive representation of the environment requires a stable hippocampal map, but the mechanisms maintaining a given map are unknown. Because sharp wave-ripples (SPW-R) orchestrate both retrospective and prospective spatial information, we hypothesized that disrupting neuronal activity during SPW-Rs affects spatial representation. Mice learned new sets of three goal locations daily in a multiwell maze. We used closed-loop SPW-R detection at goal locations to trigger optogenetic silencing of a subset of CA1 pyramidal neurons. Control place cells (nonsilenced or silenced outside SPW-Rs) largely maintained the location of their place fields after learning and showed increased spatial information content. In contrast, the place fields of SPW-R-silenced place cells remapped, and their spatial information remained unaltered. SPW-R silencing did not impact the firing rates or proportions of place cells. These results suggest that interference with SPW-R-associated activity during learning prevents stabilization and refinement of hippocampal maps.

During exploration of an environment, hippocampal place cells fire selectively in particular locations[1] (their 'place fields') and the sequential activation of groups of place fields can reliably describe the trajectory of the animal[2]. Collectively, a map-like representation built from place cells may serve a cognitive navigation mechanism[1,3]. Remarkably, entire place cell sequences activated during exploration are repeated or 'replayed' during sharp wave-ripple complexes (SPW-Rs), a network event observed in the hippocampal local field potential[4] during slow-wave sleep[5–8] and transient immobility periods of waking exploration[9–16]. It has been hypothesized that SPW-R-related replay of place cell sequences in the hippocampus mediates memory consolidation and the transfer of learned information from the hippocampus to the neocortex for long-term storage[17–19]. In support of this memory consolidation framework, experiments show that selectively interfering with SPW-Rs during sleep causes deterioration in memory performance[20,21] and recently formed spatial representations[22] (but see ref. 23). During wakefulness, SPW-Rs may have different functions. They are thought to help construct cognitive maps of the physical world[12,24,25] and are involved in the planning of future routes[11,12,14–16] ('prospective' function). Disruption of awake SPW-Rs also impairs behavioral performance[13]. Despite these findings, the relationship between awake SPW-Rs, hippocampal maps and memory consolidation remains to be clarified.

Mental navigation and spatial navigation are believed to be supported by similar neurophysiological mechanisms[26]. During learning and retrieval, memories are known to be transiently labile[27] and thus require a subsequent stabilization process[17,28]. Therefore, the question arises whether spatial representations (like memories) also need to be 'stabilized'. Recent experiments suggest that, indeed, active neuronal processes support hippocampal map stabilization, as optogenetic silencing of hippocampal neurons during exploration[29] or during sleep SPW-R[22] affects place field stability. Yet the neurophysiological mechanisms supporting the stabilization of the hippocampal map upon learning are still unknown.

We hypothesized that SPW-Rs are instrumental in stabilizing the spatial representation coded by place cells in the CA1 region of the hippocampus during learning. To examine the role of SPW-Rs in place field stabilization, we used focal optogenetic silencing of a subset of pyramidal neurons during SPW-Rs in a hippocampus-dependent spatial memory task[30]. Silenced place cells were compared with simultaneously recorded but nonsilenced place cells and with place cells silenced after a random delay following SPW-R detection. The spatial correlates of control place cells were largely maintained and showed increased spatial information content after learning. In contrast, the place fields of SPW-R-silenced neurons were altered, and their information failed to increase. Our findings support the hypothesis that SPW-R-associated neuronal activity is necessary for stabilizing and refining hippocampal place fields and, by extension, for maintaining a stable cognitive map.

RESULTS

Closed-loop focal optogenetic silencing of place cells

Mice (n = 5; four CaMKII-cre::Arch mice and one PV-cre::ChR2 mouse; **Supplementary Figs. 1** and **2**) were trained in a spatial learning task[30] (**Fig. 1**). After pretraining (3–4 d), they were implanted with silicon probes in the CA1 region (**Supplementary Fig. 1b**,**c**) and recorded during free behavior in their home cage or while performing

[1]New York University Neuroscience Institute, New York University, New York, New York, USA. [2]Tel Aviv University, Sackler Faculty of Medicine and Sagol School of Neuroscience, Department of Physiology and Pharmacology, Tel Aviv, Israel. [3]Department of Neurology, Medical Center, New York University, New York, New York, USA. [4]Center for Neural Science, New York University, New York, New York, USA. [5]Present addresses: Third Military Medical University, College of Basic Medical Sciences, Department of Physiology, Chongqing, China (B.H.) and Radboud University Nijmegen, Donders Centre for Neuroscience, Departments of Neuroinformatics and Neurophysiology, Nijmegen, Netherlands (R.E.). Correspondence should be addressed to G.B. (gyorgy.buzsaki@nyumc.org).

Received 23 August 2016; accepted 13 March 2017; published online 10 April 2017; doi:10.1038/nn.4543

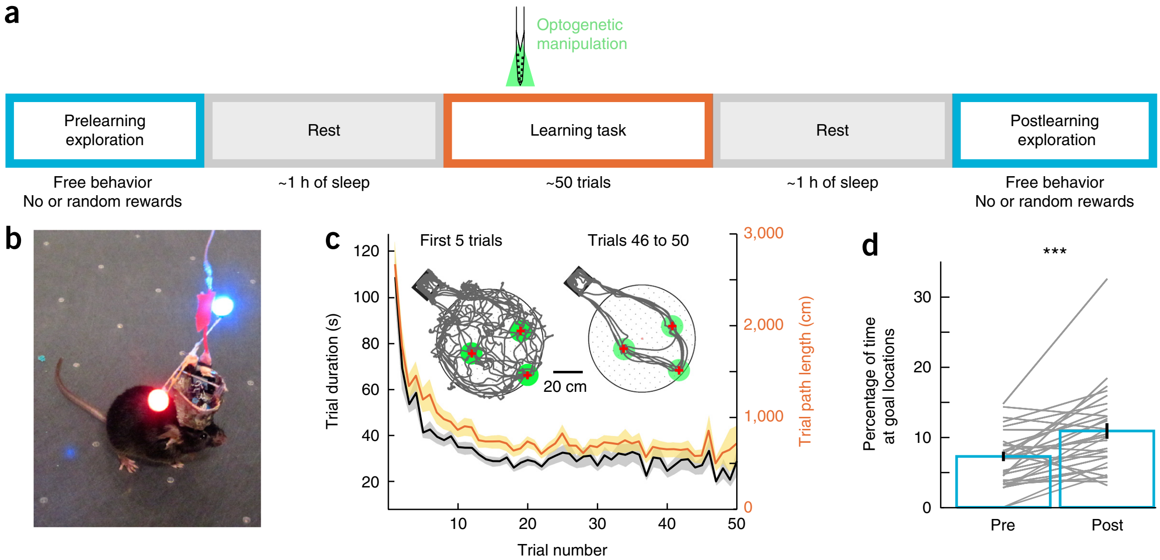

Figure 1 Daily spatial learning of hidden reward locations on the cheeseboard maze. (**a**) Five steps constituting a daily recording session[30]: prelearning exploration epoch, rest epoch in home cage, learning task, rest epoch in home cage and postlearning exploration epoch. Optogenetic manipulations were conducted during the learning task. (**b**) Implanted mouse equipped with blue and red LEDs allowing real-time position tracking. (**c**) Learning performance during the task. A new set of three baited wells was randomly selected every day but stayed fixed within a given day. Lines with shaded areas show mean ± s.e.m. for $n = 29$ sessions in 5 mice. (**d**) Mice spent consistently more time at the goal locations during the first 10 min of the postlearning exploration epoch, compared to the first 10 min of the prelearning exploration epoch (7.2 ± 0.7% and 10.8 ± 1.1% of the time for Pre and Post, respectively; $^{***}P = 0.0006$, Wilcoxon's paired signed-rank test, $n = 29$ sessions in 5 mice). Gray lines represent individual sessions.

on a 'cheeseboard' maze. Mice carried two LEDs (**Fig. 1b**), which allowed monitoring their exact location in real-time. Each session consisted of five stages (**Fig. 1a**). During the learning epoch, the mouse performed multiple trials (29–60 trials per session; median 50; $n = 29$ sessions; **Supplementary Table 1**) on the cheeseboard maze, where the mouse had to find the locations of three goal wells (baited with hidden water rewards) out of 177 possible wells. A trial was completed once the mouse had retrieved all rewards and returned to the start box to collect an additional water reward (**Fig. 1c**). The locations of the goal wells changed every day but were fixed within each day. This strategy required the mice to daily update their memory for the new goal locations in a familiar environment. Immediately before and after training, the mouse was placed back in its home cage and allowed to sleep for approximately 1 h. Memory performance and place field properties were assessed during pre- and postlearning exploration epochs, during which the mouse was allowed to explore the maze for 30 min. No rewards were available during the first 10 min, after which water drops were placed in several randomly selected wells to encourage exploration of the entire platform (Online Methods). Similarly to rats[30], the mice showed rapid daily learning and developed stereotyped and efficient trajectories after 5–10 trials (**Fig. 1c**). Memory of the newly learned goal locations was also demonstrated by the fact that mice spent significantly more time at the goal locations during the first 10 min of the postlearning epoch compared to the prelearning epoch (**Fig. 1d**; $P = 0.0006$; $n = 29$ sessions; Wilcoxon's paired signed-rank test).

During the learning epoch of the task, SPW-Rs occurred regularly at the goal locations while the animal was collecting rewards[30] (**Fig. 2d**). We hypothesized that these SPW-Rs shaped the spatial representation coded by place cells in this learning task. To test the impact of the SPW-Rs on CA1 hippocampal place fields, we used closed-loop optogenetic silencing of pyramidal cells, contingent upon real-time detection of spontaneous SPW-Rs at the goal locations. Notably, optogenetic suppression of pyramidal neuronal activity was conducted in a focal manner so that both light-responsive and control neurons could be simultaneously recorded and compared, without impacting overall hippocampus function. To deliver light focally, the recording silicon probes were equipped with etched optical fibers coupled to head-mounted laser diodes[31] (one fiber per shank; **Fig. 2a–c**) and implanted in one hemisphere ($n = 2$) or both hemispheres ($n = 3$ mice; **Supplementary Fig. 1a**). During the first rest period, we characterized the effect of light on the firing rate of each recorded neuron (100-ms light pulses; 300 pulses at 0.2 Hz; 204 ± 30 µW, mean ± s.e.m.; Online Methods). For each neuron, we defined a light-response index by comparing spiking activity between the light pulses and the preceding baseline periods (100-ms intervals starting 1 s before stimuli onset) (**Fig. 2c**, **Supplementary Figs. 3** and **4** and Online Methods). In both CaMKII-cre::Arch (direct suppression; **Fig. 2b**) and PV-cre::ChR2 mice (indirect suppression; **Supplementary Fig. 5**), focal illumination silenced most pyramidal cells recorded on the illuminated shank and occasionally some on neighboring shanks (**Fig. 2c**). Of the 1,020 putative pyramidal cells that we recorded, 402 were significantly suppressed ($P < 0.05$; Wilcoxon's paired signed-rank tests; Online Methods).

During the learning epoch, light stimuli (60-ms pulses; same light intensity as during response characterization) were triggered by online detection of spontaneous SPW-Rs to focally suppress firing of pyramidal neurons and terminate SPW-R oscillations[31] ('ripple-locked' condition; **Fig. 2d**,**e**; $n = 22$ recording sessions). This SPW-R-contingent silencing of pyramidal neurons was confined to events occurring when the head of the mouse was within the goal area, by means of real-time position tracking (**Fig. 2d**). Our SPW-R manipulation was mainly restricted to the second half of the SPW-Rs[31] (**Supplementary Fig. 6**). However, optogenetic stimulation was effective at targeting most SPW-Rs during immobility periods (82 ± 4%; Online Methods). To test for potential effects of light stimulation, not specific to SPW-R silencing, light stimuli were also delivered with a delay (100–300 ms; 60-ms pulses) relative to SPW-R detection ('ripple-delayed' condition), either in separate recording sessions ($n = 7$ sessions) or in combination with the ripple-locked condition but in the opposite

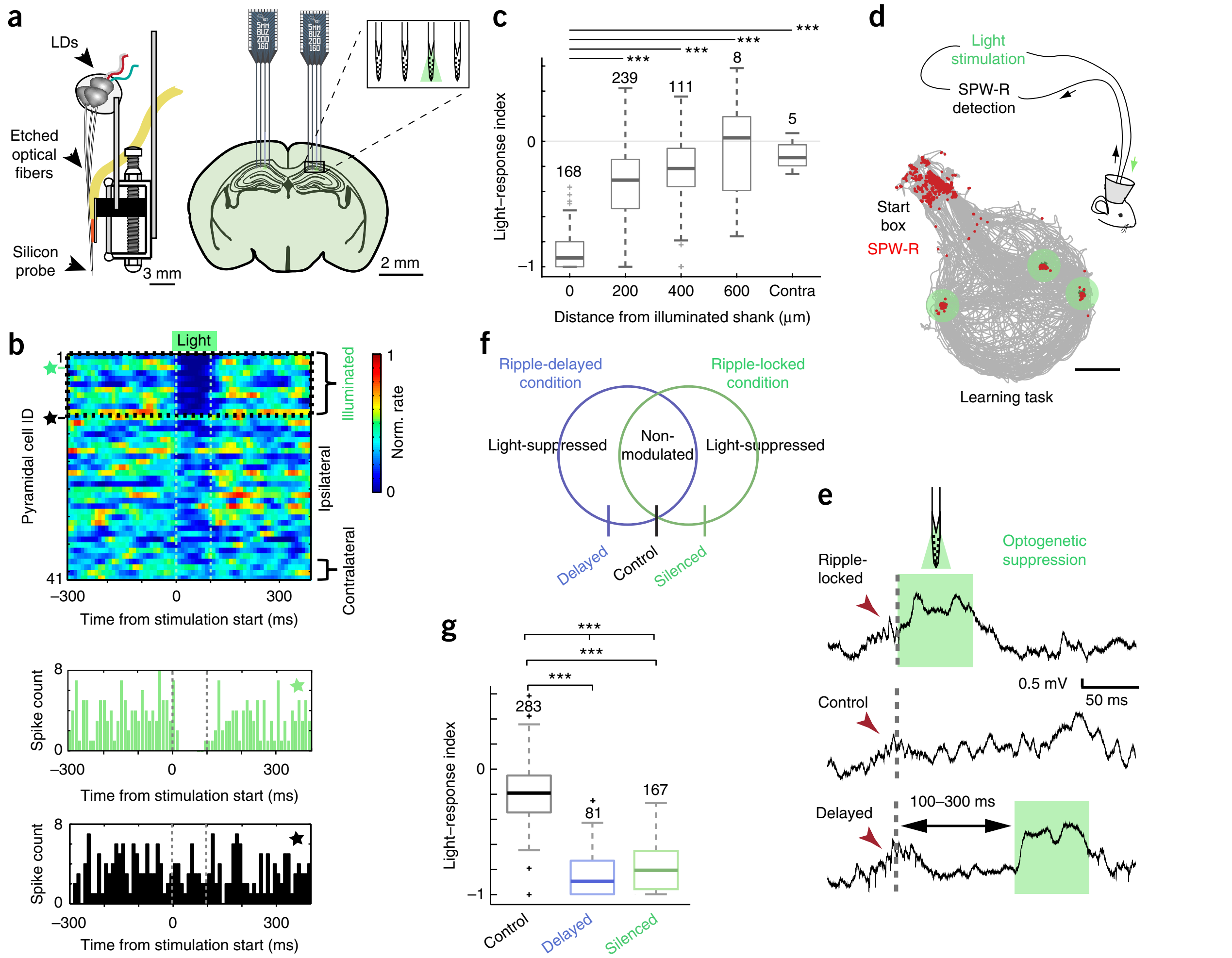

Figure 2 Closed-loop focal optogenetic silencing of pyramidal cells contingent upon SPW-R detection at goal locations. (**a**) Left: schematic of a diode-probe mounted on a movable drive. Right: diode-probes were implanted unilaterally or bilaterally in the dorsal CA1 hippocampal region. (**b**) Peristimulus histogram (PSTH) for a population of simultaneously recorded pyramidal cells, illustrating the local silencing effect provided by focal light delivery: units recorded on the illuminated shank (top; black dotted line box) are strongly suppressed during illumination. Below are shown examples of PSTHs for a light-suppressed (green star in top panel) and a Control (black star in top panel) pyramidal cell. (**c**) Light-response indices as a function of distance from illuminated shank. The number of place cells recorded at each distance is shown above boxes. Indices: –0.88 ± 0.01 (0 μm), –0.34 ± 0.02 (200 μm); –0.24 ± 0.02 (400 μm); –0.06 ± 0.15 (600 μm); –0.11 ± 0.05 (contralateral hemisphere). Kruskall-Wallis test: $***P = 2.4 \times 10^{-64}$; Tukey's *post hoc* tests: neurons from illuminated shank vs. 200-μm neurons, $***P = 9.91 \times 10^{-9}$; vs. 400-μm neurons, $***P = 9.91 \times 10^{-9}$; vs. 600-μm neurons, $***P = 1.05 \times 10^{-7}$; vs. contralateral neurons, $***P = 2.00 \times 10^{-5}$; $P > 0.05$ for all other comparisons; $n = 531$ place cells). (**d**) Offline detected SPW-Rs (red dots) are displayed on top of the animal's trajectory (gray) for an example learning session. Note that SPW-Rs mainly occur at the goal locations (green disks) and in the start box. 86 ± 2% of all SPW-Rs occurred in the start box (where the mouse stayed mostly immobile; $n = 7$ sessions). Light stimuli (60 ms) were only triggered by SPW-Rs in the goal areas (green disks). (**e**) Light stimuli aborted ripples locally (top) but had no effect in control (nonilluminated shank, middle) and delayed (bottom) condition. The positive deflections in the extracellular signal during light stimuli reflect physiological neuronal hyperpolarization[44]. (**f**) Schematic illustrating place cell classification into three categories based on experimental model (optogenetic stimulation triggered with or without delay relative to SPW-R detection) and their firing rate modulation by light (Online Methods). (**g**) Optogenetic silencing effect in the three groups of place cells (indices: –0.20 ± 0.01, Control; –0.84 ± 0.02, Delayed; –0.78 ± 0.02, Silenced; Kruskall-Wallis test: $***P = 2.6 \times 10^{-78}$; Tukey's *post hoc* tests: Control vs. Delayed, $P = 0.52$; Control vs. Silenced, $***P = 9.56 \times 10^{-10}$; Delayed vs. Silenced, $***P = 9.56 \times 10^{-10}$; $n = 283$, 81 and 167 Control, Delayed and Silenced place cells). In box plots, the central mark indicates the median and the bottom and top edges of the box indicate the 25th and 75th percentiles, respectively. Whiskers extend to the most extreme data points not considered outliers, and the outliers are plotted individually.

hemisphere ($n = 9$ sessions). Behavioral performance (measured by the proportion of time spent in goal areas in the postlearning exploration (Post) compared to the prelearning exploration (Pre) epoch; **Fig. 1d**) was identical regardless of whether a ripple-locked or a ripple-delayed condition was employed during the learning task ($P = 0.7$; Mann-Whitney U test on the differences Post – Pre; $n = 7$ ripple-delayed and $n = 13$ ripple-locked sessions; **Supplementary Fig. 7**).

Of the 1,406 units recorded in 29 sessions, 227 were classified as putative interneurons and 1,020 as putative pyramidal cells (Online Methods and **Supplementary Fig. 3a**). Of the putative pyramidal cells, 637 had a place field on the cheeseboard maze in a least one of the two exploration epochs (Pre and/or Post; Online Methods). For quantitative analyses, we used two approaches. In the first approach, place cells that were silenced by light pulses in the ripple-locked condition were referred to as 'Silenced', whereas place cells silenced in the ripple-delayed condition were referred to as 'Delayed'. Place cells that were unaffected by light pulses in both of these stimulation conditions were defined as Control (**Fig. 2f,g**). Of the 637 place cells, 106 were discarded because they did not

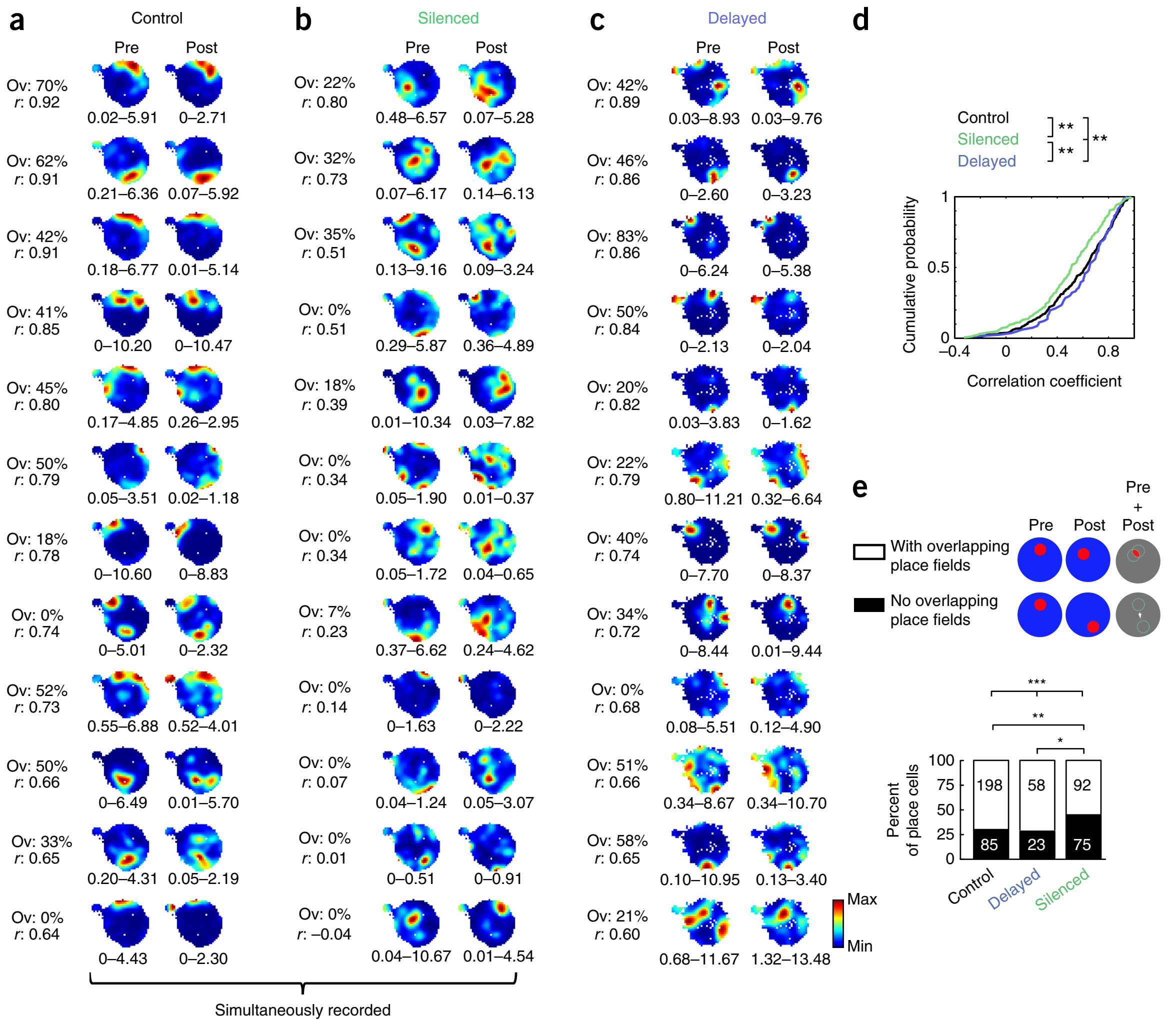

Figure 3 Silencing pyramidal neurons during SPW-Rs impairs place map stability of place cells. (**a**–**c**) Examples of firing rate maps obtained from the Pre and Post exploration epochs in example sessions for individual (**a**) Control, (**b**) Silenced and (**c**) Delayed place cells. The correlation coefficient (*r*), calculated by comparing firing rate maps in Pre and Post exploration epochs, and the percentage of overlap (Ov) between the place fields detected in these two epochs are shown for each place cell on the left. 0% overlap indicates shifting place fields ('no overlapping place fields' in **e**). Twelve place cells with the highest *r* values in each category are depicted. Control and Silenced place cells (**a** and **b**) were recorded during the same session. (**d**) Cumulative distributions of the *r* values obtained for individual place cells in the three groups. Kruskall-Wallis test: $**P = 0.002$, all three groups; Tukey's *post hoc* tests: $**P = 0.008$, Control vs. Silenced; $**P = 0.007$, Delayed vs. Silenced; $P = 0.62$, Control vs. Delayed; $n = 283$ Control, $n = 81$ Delayed and $n = 167$ SPW-R Silenced place cells. (**e**) Proportions of place cells with shifting fields (no overlapping place fields, black) or overlapping place fields (white) in the three groups of place cells. The number of cells in each category is indicated on the bars (χ^2 test: $***P = 5.8 \times 10^{-4}$; *post hoc* two-sided Fisher's exact tests followed by Bonferroni correction: $**P = 0.004$, Control vs. Silenced; $*P = 0.04$, Delayed vs. Silenced; $P = 1$, Control vs. Delayed).

meet our criteria for classification (Online Methods and **Supplementary Table 1**). Of the 531 remaining place cells, 167 were assigned to the Silenced group, 81 to the Delayed group and 283 to the Control group (**Fig. 2g**). Because silencing of pyramidal neurons may bring about local circuit effects[3], we also used an alternative categorization, in which we grouped place cells based on the type of intervention done (either ripple-locked or ripple-delayed), independently of the magnitude of their responses to light. The two groups in this second approach were referred to as 'ripple-locked' and 'ripple-delayed' place cells ($n = 385$ and $n = 247$ place cells, respectively).

Perturbation of SPW-R-associated neuronal activity destabilizes place fields

The stability of the hippocampal spatial map was examined by comparing recordings from the Pre and Post exploration epochs in the Control, Silenced and Delayed groups of place cells. No light stimulation was administered during these epochs. **Figure 3a**–**c** illustrates representative rate maps for Control, Silenced and Delayed place cells. For each place cell, we calculated the pixel-by-pixel Pearson correlation coefficient between the rate maps obtained from the Pre and Post epochs to quantify the stability of the spatial representation. By comparing the resulting correlation coefficients across the Control, Silenced and Delayed groups, we found that optogenetic silencing of pyramidal neurons during SPW-Rs reduced the stability of the rate map compared to Control neurons (**Fig. 3d**). In contrast, delayed suppression of place cells had no consistent effect (mean correlation coefficient ± s.e.m.: 0.56 ± 0.02; 0.60 ± 0.03 and 0.49 ± 0.02 for Control, Delayed and Silenced ensembles, respectively; overall group effect, Kruskall-Wallis test, $P = 0.002$; Tukey's *post hoc* tests: Silenced versus Control, $P = 0.008$; Silenced versus Delayed, $P = 0.007$; Delayed versus Control, $P = 0.62$). We also quantified the proportion of place cells that shifted their place fields so that

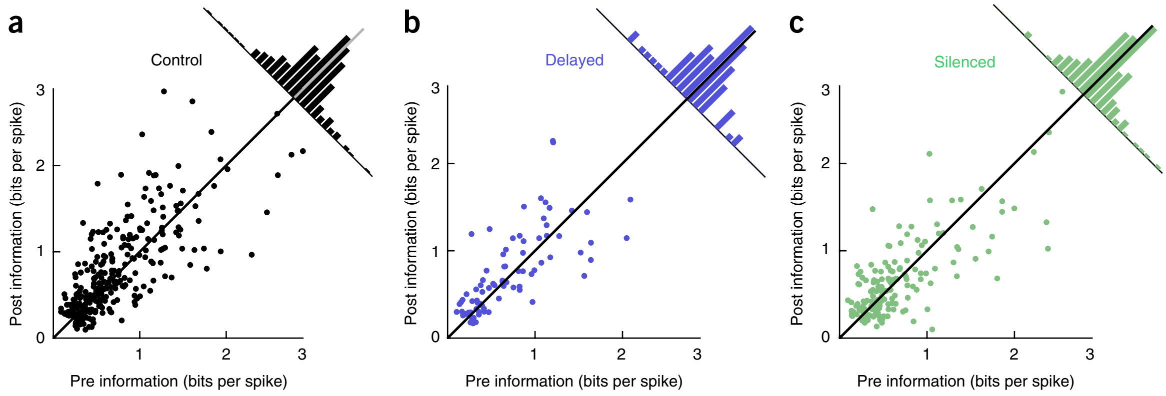

Figure 4 SPW-R silencing impact information measures of place cells. (**a**–**c**) Distributions of 'information content' values carried by place cells during Pre and Post exploration epochs. While (**a**) Control place cells showed increased information content, the information content of (**c**) Silenced place cells remained similar across Pre and Post exploration epochs (0.68 ± 0.04 and 0.67 ± 0.04 bits per spike for Pre and Post, respectively; Wilcoxon's paired signed rank test: $P = 0.86$; $n = 167$ SPW-R Silenced place cells; Control group: 0.74 ± 0.03 and 0.80 ± 0.03 bits per spike for Pre and Post, respectively; Delayed group: 0.70 ± 0.05 and 0.75 ± 0.05 bits per spike; $^{**}P = 0.007$, $P = 0.13$ for Control and Delayed groups, respectively; $n = 283$ Control and $n = 81$ Delayed place cells). Two outlier values in the Silenced and Control groups are not displayed but included in the statistical analyses (their exclusion does not affect the conclusions).

their fields did not overlap between the Pre and Post exploration epochs (**Fig. 3e** and Online Methods). The majority of Control and Delayed neurons preserved their place fields, as only a small fraction of neurons (Control group: 85 of 283, 30%; Delayed group: 23 of 81, 24%) showed non-overlapping place fields. In contrast, a larger fraction of neurons shifted their place preference in the Silenced group (75 of 167, 45%; $P = 5.8 \times 10^{-4}$, χ^2 test for three groups; Silenced versus Control, $P = 0.004$; Silenced versus Delayed, $P = 0.04$; Delayed versus Control, $P = 1$; two-tailed Fisher's exact test with Bonferroni correction; **Supplementary Fig. 8**).

In the second approach, which categorized place cells by the type of perturbation (ripple-locked versus ripple-delayed conditions), the pixel-by-pixel Pearson correlation between the rate maps obtained from the Pre and Post exploration epochs was significantly different between the ripple-locked and the ripple-delayed groups ($n = 385$ and $n = 247$ place cells, respectively; $P = 0.007$; Mann-Whitney U test; **Supplementary Fig. 9h**). We found no reliable correlation between the light response indices of individual place cells and their stability, as assessed by the correlation coefficient of their Pre and Post rate maps (**Supplementary Fig. 9i**). This observation suggests that map stability largely depends on the timing of neuronal suppression relative to SPW-Rs (locked versus Delayed). However, among the ripple-locked place cells, but not among ripple-delayed neurons, those that switched their place field preference (no overlapping place fields between Pre and Post explorations) were more strongly suppressed by light as compared to nonswitching place cells (**Supplementary Fig. 9k**,**l**). This result indicates that the most strongly suppressed cells in the ripple-locked group showed the largest place field shifts. This observation is in line with results from the first approach, which demonstrated that SPW-R-suppressed (Silenced) place cells had less stable place fields than nonsuppressed (Control) place cells. Both approaches show that suppressing neuronal activity during SPW-Rs at the goal locations altered the place maps of many place cells, with the largest impact on the most strongly suppressed ones. Overall, this result further confirms that activity during SPW-Rs is necessary for stabilizing place fields of pyramidal neurons.

Notably, differences in place field stability across the Silenced, Control and Delayed groups observed with the first approach could not be explained by mean or peak firing-rate differences, since these values did not differ across groups or between the Pre and Post epochs (**Supplementary Fig. 10b**,**c**). One could also hypothesize that Silenced neurons would lose their initial place fields and not even be classified as place cells in Post. However, the three groups showed similar proportions of neurons that lost and gained place fields between the Pre and Post exploration epochs (**Supplementary Fig. 10e**,**f**). Similarly, ripple-locked and ripple-delayed neurons defined via the second approach did not differ from each other in terms of firing rates or proportions of place cells (**Supplementary Fig. 9b**–**e**). Moreover, place cell remapping was not related to measures of recording instability (**Supplementary Fig. 11a**–**d**). These observations indicate that although Silenced individual place cells changed their spatial representation following SPW-R silencing, they still effectively carried spatial information.

SPW-R-triggered pyramidal cell silencing impairs place map refinement

SPW-R silencing could also impact the amount of spatial information carried by place cells. To explore this possibility, we compared the information content (bits per spike) carried by each place cell between the Pre and Post epochs (**Fig. 4**). We found that place cells in the Control group carried more spatial information per spike in the Post epoch compared to Pre (**Fig. 4**a; $P = 0.007$, Wilcoxon's paired signed-rank test; $n = 283$). In contrast, the information content of Silenced place cells did not increase significantly from Pre to Post (**Fig. 4c**; $P = 0.86$; $n = 167$). Related measures of place field features followed a similar trend: sparsity decreased and selectivity increased between the Pre and Post epochs in the Control group (sparsity, $P = 0.01$; selectivity, $P = 0.04$). In contrast, these measures remained unchanged in the Silenced group (sparsity, $P = 0.97$; selectivity, $P = 0.44$). Notably, the information content carried by place cells was similar across the experimental groups in the Pre epoch (i.e., before optogenetic manipulation; Kruskall-Wallis test, $P = 0.18$; 0.74 ± 0.03, 0.70 ± 0.05 and 0.68 ± 0.04 for Control, Delayed and Silenced groups, respectively). Using the second approach, we confirmed that in the ripple-delayed group, spatial information per spike increased significantly in the Post epoch compared to Pre ($P = 0.00007$; $n = 247$; Wilcoxon's paired signed-rank test), whereas no difference was detected in the ripple-locked group ($P = 0.49$; $n = 385$; **Supplementary Fig. 9f**,**g**). Overall, these observations suggest that the activity associated with SPW-Rs surrounding reward consumption contributed to the refinement of the cognitive map coded by place cells.

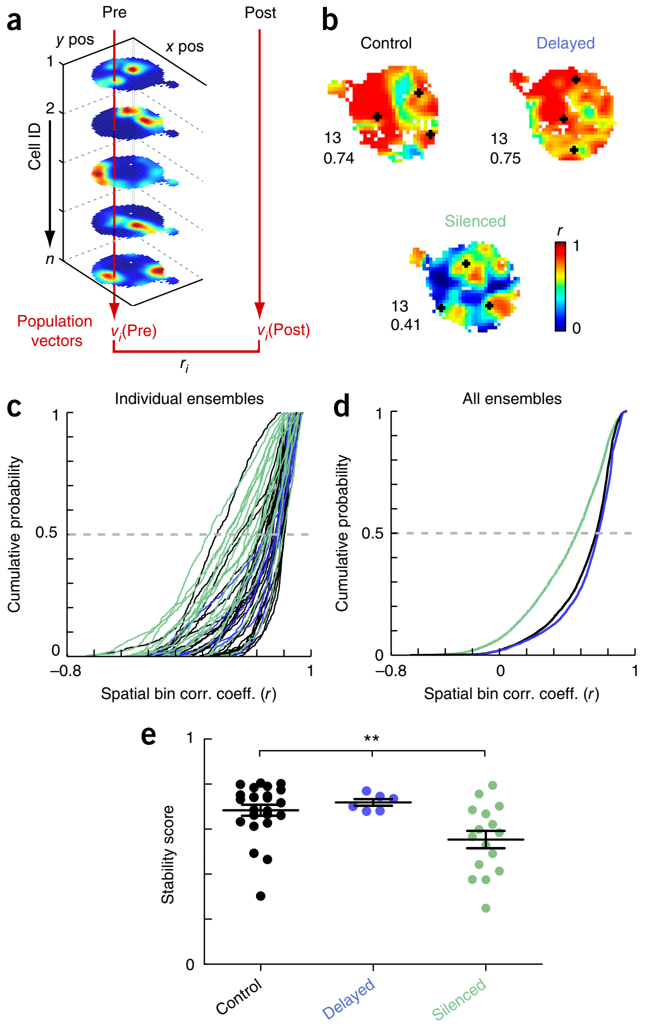

Figure 5 Silencing neurons during SPW-Rs impairs place map stability of place cell ensembles. (**a**) Schematic illustrating population vector analysis method. For each spatial bin i, a population vector v_i was constructed containing the rates in bin i for each cell of the ensemble. This was done for all spatial bins, separately for the rate maps of the Pre and Post exploration epochs. Then, for each spatial bin i, the Pearson correlation (r_i) between v_i(Pre) and v_i(Post) was computed. r_i indicates the stability of the ensemble spatial representation at pixel i. Correlation maps were constructed by assigning the r values to their respective positions along the x and y axes. (**b**) Examples of correlation maps obtained for ensembles of Control, Delayed and Silenced place cells. Correlation values of individual spatial bins (r) are color coded. The number of cells comprising the ensemble and the stability score, defined as the median of all bins' correlation values (r), are indicated on the left of each map. Goal locations are indicated by black crosses. (**c**) Cumulative distribution of population correlation values across spatial bins for individual ensembles of place cells. $n = 24$ Control (black), 6 Delayed (blue) and 16 Silenced (green) ensembles of place cells. (**d**) Cumulative distributions of the correlation values accumulated for all ensembles of place cells from the three groups. (**e**) Stability scores for the individual ensembles of place cells shown in **c** (Kruskall-Wallis test: $^{**}P = 0.009$; Tukey's *post hoc* tests: $^{*}P = 0.013$, Control vs. Silenced; $P = 0.94$, Control vs. Delayed; $P = 0.068$, Delayed vs. Silenced). Error bars indicate s.e.m.

Perturbation of SPW-R-associated activity results in destabilized spatial representations of place cell ensembles

In the hippocampus, the representation of each spatial location relies on the coordinated activity of multiple neurons[2]. We thus tested whether optogenetic SPW-R-triggered pyramidal cell silencing during learning impacts the stability of the spatial representation at the population level, mirroring the effects we saw at the level of individual place cells. The stability of the spatial representation coded by ensembles of place cells was quantified by a population vector analysis[30,32] (**Fig. 5a–d**). For each ensemble of simultaneously recorded place cells ($n = \geq 5$ place cells in each ensemble; range: 5–28; **Supplementary Table 1**), the median correlation coefficient (computed across all pixels between the Pre and Post exploration epochs) was defined to as a 'stability score'. This measure provided an estimate of the consistency of the spatial representation at the neuronal ensemble level ($n = 24$, $n = 6$ and $n = 16$ ensembles for Control, Delayed and Silenced ensembles, respectively; **Supplementary Table 1**). Stability scores differed between the three groups (stability scores: 0.68 ± 0.02; 0.72 ± 0.02 and 0.55 ± 0.03 for Control, Delayed and Silenced ensembles, respectively; $P = 0.009$; Kruskall-Wallis test; **Fig. 5e**): Silenced assemblies showed lower stability scores than the Control and Delayed ensembles (*post hoc* Tukey's tests; $P = 0.01$, for Control versus Silenced; $P = 0.07$ for Delayed versus Silenced; $P = 0.94$ for Control versus Delayed). Using the neuron assignment of the second approach, we also observed a consistent difference between the stability scores of ripple-delayed and ripple-locked place cell ensembles ($P = 0.009$; $n = 19$ ripple-locked and 12 ripple-delayed ensembles; Mann-Whitney U test; **Supplementary Fig. 9m–o**).

To control for the possibility that the aforementioned ensemble destabilization effect of SPW-R-triggered silencing was due to intersession variability in the stability of place cell ensembles, we performed within-session comparisons. On some recording days, we recorded from sufficient numbers of neurons to allow comparison between Silenced and Control or Delayed and Control neuron ensembles in the same mouse ($n = 15$ sessions with Control and Silenced ensembles; $n = 6$ sessions with Control and Delayed ensembles; **Fig. 6a**). In 12 of the 15 Control–Silenced sessions, the stability score was higher in the Control compared to the simultaneously recorded Silenced ensemble ($P = 0.02$; Wilcoxon's paired signed-rank test) (**Fig. 6b**). In contrast, the Delayed ensembles showed both higher and lower stability scores than the simultaneously recorded Control ensembles, and no group effect was observed ($P = 0.84$; **Fig. 6b**). The stability score differences between the pairs of simultaneously recorded ensembles was larger for Control–Silenced pairs than for Control–Delayed pairs (**Fig. 6c**; $P = 0.05$; Mann-Whitney U test). Similar results were obtained after controlling for ensemble size (**Supplementary Fig. 12** and Online Methods). These within-session differences between Control and manipulated place cell populations present further evidence that activity during awake SPW-R of learning promotes stabilization of place representation coded by hippocampal neuron ensembles.

SPW-R perturbation does not affect place field stability in a cue-guided task

Following the main experiment, mice were trained in a cue-guided task, in which the goal locations were signaled by local cues placed next to the three baited wells. In this 'cued' version of the task, mice could rely on the cues to find the rewards instead of depending on memorized internal representation of goal locations[30], resulting in a flat learning curve (**Supplementary Fig. 13a**; $n = 10$ sessions in 4 mice). Closed-loop SPW-Rs disruption pyramidal cell activity was conducted in those experiments, as for the noncued version of the task. Place fields were significantly more stable than in the noncued version of the task and, notably, they were not affected by optogenetic disruption of SPW-R at the goal locations (**Supplementary Fig. 13b**). This observation suggests that neuronal silencing

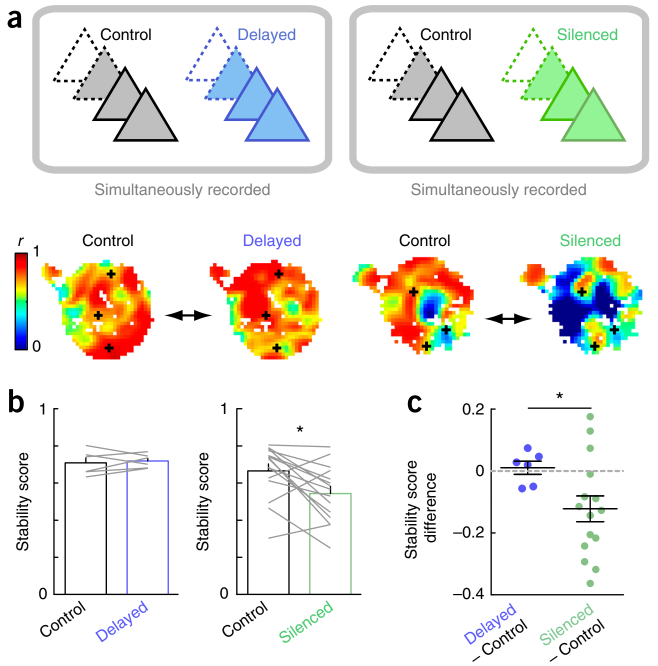

Figure 6 SPW-R Silenced ensembles of place cells show destabilized spatial representation as compared to simultaneously recorded Control ensembles. (**a**) Top: schematic illustrating the method used for within-session comparison of place cell ensemble pairs. Bottom: examples of correlation maps for pairs of ensembles, simultaneously recorded within the same session (left, ensembles of Control and Delayed place cells; right, ensembles of Control and Silenced place cells). (**b**) Left: ensembles of Delayed place cells show stability scores similar those of to their matched Controls from the same recording session (scores: 0.71 ± 0.03 and 0.72 ± 0.02 for Control and Delayed ensembles, respectively; Wilcoxon's paired signed-rank test: $P = 0.84$, $n = 6$ pairs). Right: in contrast, ensembles of Silenced place cells show lower stability scores compared to their matched Control ensembles (scores: 0.67 ± 0.04 and 0.54 ± 0.04 for Control and Silenced ensembles, respectively; $^*P = 0.015$, $n = 15$ pairs). (**c**) Within-session differences between the stability scores of optogenetically manipulated ensembles and their matched Control ensembles (0.01 ± 0.02 for Delayed–Control pairs and –0.12 ± 0.04 for Silenced–Control pairs; Mann-Whitney U test: $^*P = 0.047$). Dashed gray line indicates zero level (no difference). Error bars indicate s.e.m.

during SPW-Rs per se does not affect the hippocampal map in absence of memory requirements.

Place cell silencing during awake SPW-Rs does not impact their activity during SPW-R of slow-wave sleep

To test whether our manipulation of awake SPW-Rs had an impact on sleep SPW-Rs, we analyzed the activity of place cells during the SPW-Rs of slow-wave sleep, detected during the rest periods in the home cage preceding and following learning. First, we compared the changes in firing rates, participation, spike count and gain between the prelearning and postlearning SPW-Rs of slow-wave sleep, across the three groups of place cells (Control, Delayed and Silenced). No differences were found between these groups (**Supplementary Fig. 14a**), indicating that SPW-R suppression of pyramidal neurons during waking did not impact the activity of neurons during sleep SPW-Rs[13], at least for the parameters that we considered. Furthermore, we did not detect any reliable relationship between changes in SPW-R activity (rate, participation, spike count or gain) and place map stability of individual place cells (**Supplementary Fig. 14b–e**), suggesting that those parameters did not predict the magnitude of remapping of place cells. Yet our results do not rule out the possibility that, using a considerably larger data set and more sophisticated analyses, place cell silencing may exert an impact on sleep SPW-R content.

DISCUSSION

During exploration, two distinct classes of behaviors alternate: preparatory behaviors, including locomotion of the animal from place to place (foraging), and consummatory behaviors, including transient immobility and food and/or water consumption[33]. These two behavioral classes are respectively associated with theta and SPW-R patterns in the hippocampus[18,34]. One hypothesized role of consummatory states is to maintain the cognitive map[26] and to prepare the animal to calculate new routes in a familiar environment[24,35]. In our experiments, SPW-Rs occurred regularly at the goal locations when the animal momentarily stopped and drank water. Aborting the buildup of SPW-Rs by optogenetic means at the reward locations reduced place field stability tested across Pre and Post epochs. This was expressed by the reduced correlation of place fields at both the single neuron level and the population level, place field shifts, impaired spatial information content of spikes and related measures, without any effect on firing rates. Notably, our selective, focal optogenetic perturbations suppressed spiking in only a small group of pyramidal cells with minimal effects on neighboring networks and without affecting memory performance. Our findings suggest that the small number of place cells Silenced during SPW-Rs were 'left out' of the ongoing map stabilization process. Overall, these results support the hypothesis that SPW-Rs promote the maintenance of the cognitive map[12,24].

SPW-Rs and stabilization of the hippocampal map

The stability of the cognitive map may deteriorate spontaneously or be modified by various perturbations. Rats re-entering the same environment have been tacitly assumed to have stable spatial maps[1,36]. However, recent experiments suggest that the cognitive map destabilizes over time[32,37]. Moreover, firing rates and place field sizes undergo changes during the first few trials, even after repeated exposure to the same familiar environment[38]. During these early trials the running speed is typically slow, and the animal often rears, 'scans' the environments[39] and stops frequently. SPW-Rs during such immobility periods may be instrumental in maintaining the cognitive map[12,24]. In our experiments, distal environmental cues and the maze itself remained unchanged from day to day and therefore, in principle, no novel construction of the spatial map was needed. Yet it is possible that learning and recalling the new goal locations contributed to a destabilization of the hippocampal map[40], supporting the view that incorporating new information in pre-existing knowledge[41] (a 'schema') necessitates a reconsolidation process[28]. Our experiments showing that Control place fields were more stable in the cue-guided task than in the noncued ('memory') version of the task are in line with this theory (**Supplementary Fig. 13b**). Our observation that optogenetic disruption of place cell activity during awake SPW-Rs at the goal locations affected their spatial representation in the memory version of the task, but not in the cue-guided version of the task, further suggests that SPW-Rs may be involved in the reconsolidation process. The idea that SPW-Rs have a 'stabilizing' role in specific conditions of memory requirements is also supported by the fact that place fields remain stable in a well-learned working memory task, despite SPW-Rs disruption[13]. Complementary to our findings, recent experiments show that global and extended silencing of CA1 neurons during exploration[29] or during SPW-Rs of sleep following exploration of a novel environment affect place field stability[22] (but see ref. 23). On the basis of these findings, we hypothesize that neuronal activity during awake SPW-Rs is important for hippocampal map stabilization when new configurations within the map are learned.

Learning performance observed in mice was comparable to that of rats trained in a similar task[30]. However, in contrast to rats[30], we did not observe a goal-related reorganization of place fields (**Supplementary Fig. 15**). The correlation maps obtained by population vector analysis of SPW-R-silenced place cells did not show any consistent spatial pattern with regards to goal locations or other locations in the maze (**Figs. 5** and **6**), and the probability of a place cell to fire at goal areas did not predict the magnitude of its place field change (**Supplementary Fig. 11e**). These observations suggest that SPW-R silencing did not impact the representation of specific regions of the environment. Instead, representation of any location of the maze had a similar chance of being affected. We therefore hypothesize that participation in SPW-Rs contributes to the global maintenance of a singular map of the environment.

Mechanisms of SPW-R-assisted maintenance of place maps

In novel or changing environments, CA1 and CA3 neurons remap at different rates[30,32,42,43]. Notably, CA3 place fields are more stable than CA1 place fields across repeated exposures to the same environment[30,32,43]. Since CA3 constitutes the major drive to CA1 during SPW-Rs[4], SPW-Rs may be responsible for restoring a coherent representation between CA3 and CA1 regions.

Alternatively, SPW-Rs may stabilize and refine CA1 place fields through a local impact on CA1 circuits. Indeed, ample evidence suggests the importance of local processing within the CA1 region. Whereas the CA3 drive can contribute to the sequential firing of CA1 neurons during SPW-Rs, CA1 sequences can be also supported by local interactions between pyramidal cells and interneurons[44], indicating CA3 input-independent coordination in CA1 circuits. Local inhibition may shape the composition of cell assemblies for specific regions of space[3,29], and changes in interneuron networks have been shown to mirror place field reorganization during learning in CA1 (ref. 45). These data suggest that the place map in CA1 is not simply inherited from upstream regions, and important contributions from local processing may participate in map stability.

Results from the ripple-delayed control group and from the cue-guided version of the task demonstrate that transient optogenetic hyperpolarization per se does not affect CA1 place fields. Indeed, we did not find consistent differences between the nonlight-modulated Control and the Delayed place cells in any stability measure. Furthermore, optogenetic hyperpolarization during SPW-Rs at goal locations in a control cue-guided task did not affect place field stability (**Supplementary Fig. 13b**). These control experiments suggest that optogenetic hyperpolarization does not induce a destabilization but rather prevents a stabilization process from occurring during SPW-Rs in the context of learning. The plasticity mechanisms associated with SPW-Rs (which would support such stabilization) remain to be understood. During SPW-Rs, spiking activity of CA1 neurons coincides with their organized CA3 inputs: dendritic spikes may be induced and somadendritic back-propagation of spikes facilitated[46]. The coincidence of back-propagating spikes and the excitatory postsynaptic currents evoked by the spike-inducing inputs has been shown to induce synaptic plasticity[47]. Dendritic subthreshold activity during SPW-Rs could also support plasticity in the absence of somatic action potentials[48,49]. In our study, optogenetic hyperpolarization of pyramidal neurons during SPW-Rs could have impacted these potential plasticity mechanisms, preventing the stabilization of the hippocampal map. Reward consumption is associated not only with SPW-Rs in the hippocampus but also with spike bursts in dopaminergic neurons of the ventral tegmental area[50]. The reward-induced temporal correlation between enhanced dopaminergic activity and SPW-R-related population bursts in the hippocampus may contribute to the place cell stabilization process.

Overall, our observations suggest that SPW-Rs represent specific time windows during which neurons engage in plasticity mechanisms essential for maintaining and refining cognitive maps. These physiological findings demonstrate why it is beneficial for ambulatory movements to be interrupted by consummatory actions during exploration and learning. Furthermore, they provide mechanistic insights into why SPW-R-related activity supports memory function.

METHODS

Methods, including statements of data availability and any associated accession codes and references, are available in the online version of the paper.

Note: Any Supplementary Information and Source Data files are available in the online version of the paper.

ACKNOWLEDGMENTS

We thank N. Chenouard, G. Girardeau, L. Sjulson, A. Peyrache and all members of the lab for invaluable discussions, advice and comments on the manuscript. This work was supported by NIH grants MH107396, MH54671, U01NS090583, the Simons Foundation, and the G. Harold and Leila Y. Mathers Foundation. L.R. was supported by the NIH grant K99NS094735 and the Bettencourt Schueller Foundation. E.S. was supported by the Rothschild Foundation, Human Frontiers in Science Program LT-000346/2009-l, Machiah Foundation 20090098 and ERC-2015-StG 679253. B.H. was supported by the National Natural Science Foundation of China (grant no. 31471050).

AUTHOR CONTRIBUTIONS

L.R. and G.B. designed the experiments and wrote the manuscript; L.R. performed the experiments and analyzed the data; B.H. performed experiments; R.E. provided the software for online tracking of mouse position; and E.S. provided assistance for data analysis.

COMPETING FINANCIAL INTERESTS

The authors declare no competing financial interests.

1. O'Keefe, J. & Nadel, L. *The Hippocampus as a Cognitive Map* (Oxford University Press, 1978).
2. Wilson, M.A. & McNaughton, B.L. Dynamics of the hippocampal ensemble code for space. *Science* **261**, 1055–1058 (1993).
3. Trouche, S. *et al.* Recoding a cocaine-place memory engram to a neutral engram in the hippocampus. *Nat. Neurosci.* **19**, 564–567 (2016).
4. Buzsáki, G., Leung, L.W. & Vanderwolf, C.H. Cellular bases of hippocampal EEG in the behaving rat. *Brain Res.* **287**, 139–171 (1983).
5. Wilson, M.A. & McNaughton, B.L. Reactivation of hippocampal ensemble memories during sleep. *Science* **265**, 676–679 (1994).
6. Kudrimoti, H.S., Barnes, C.A. & McNaughton, B.L. Reactivation of hippocampal cell assemblies: effects of behavioral state, experience, and EEG dynamics. *J. Neurosci.* **19**, 4090–4101 (1999).
7. Nádasdy, Z., Hirase, H., Czurkó, A., Csicsvari, J. & Buzsáki, G. Replay and time compression of recurring spike sequences in the hippocampus. *J. Neurosci.* **19**, 9497–9507 (1999).
8. Lee, A.K. & Wilson, M.A. Memory of sequential experience in the hippocampus during slow wave sleep. *Neuron* **36**, 1183–1194 (2002).
9. Foster, D.J. & Wilson, M.A. Reverse replay of behavioural sequences in hippocampal place cells during the awake state. *Nature* **440**, 680–683 (2006).
10. Csicsvari, J., O'Neill, J., Allen, K. & Senior, T. Place-selective firing contributes to the reverse-order reactivation of CA1 pyramidal cells during sharp waves in open-field exploration. *Eur. J. Neurosci.* **26**, 704–716 (2007).
11. Diba, K. & Buzsáki, G. Forward and reverse hippocampal place-cell sequences during ripples. *Nat. Neurosci.* **10**, 1241–1242 (2007).
12. Gupta, A.S., van der Meer, M.A., Touretzky, D.S. & Redish, A.D. Hippocampal replay is not a simple function of experience. *Neuron* **65**, 695–705 (2010).
13. Jadhav, S.P., Kemere, C., German, P.W. & Frank, L.M. Awake hippocampal sharp-wave ripples support spatial memory. *Science* **336**, 1454–1458 (2012).
14. Pfeiffer, B.E. & Foster, D.J. Hippocampal place-cell sequences depict future paths to remembered goals. *Nature* **497**, 74–79 (2013).

15. Singer, A.C., Carr, M.F., Karlsson, M.P. & Frank, L.M. Hippocampal SWR activity predicts correct decisions during the initial learning of an alternation task. *Neuron* **77**, 1163–1173 (2013).
16. Papale, A.E., Zielinski, M.C., Frank, L.M., Jadhav, S.P. & Redish, A.D. Interplay between hippocampal sharp-wave-ripple events and vicarious trial and error behaviors in decision making. *Neuron* **92**, 975–982 (2016).
17. Buzsáki, G. Two-stage model of memory trace formation: a role for "noisy" brain states. *Neuroscience* **31**, 551–570 (1989).
18. Buzsáki, G. Hippocampal sharp wave-ripple: A cognitive biomarker for episodic memory and planning. *Hippocampus* **25**, 1073–1188 (2015).
19. Sutherland, G.R. & McNaughton, B. Memory trace reactivation in hippocampal and neocortical neuronal ensembles. *Curr. Opin. Neurobiol.* **10**, 180–186 (2000).
20. Girardeau, G., Benchenane, K., Wiener, S.I., Buzsáki, G. & Zugaro, M.B. Selective suppression of hippocampal ripples impairs spatial memory. *Nat. Neurosci.* **12**, 1222–1223 (2009).
21. Ego-Stengel, V. & Wilson, M.A. Disruption of ripple-associated hippocampal activity during rest impairs spatial learning in the rat. *Hippocampus* **20**, 1–10 (2010).
22. van de Ven, G.M., Trouche, S., McNamara, C.G., Allen, K. & Dupret, D. Hippocampal offline reactivation consolidates recently formed cell assembly patterns during sharp wave-ripples. *Neuron* **92**, 968–974 (2016).
23. Kovács, K.A. *et al.* Optogenetically blocking sharp wave ripple events in sleep does not interfere with the formation of stable spatial representation in the CA1 area of the hippocampus. *PLoS One* **11**, e0164675 (2016).
24. Samsonovich, A.V. & Ascoli, G.A. A simple neural network model of the hippocampus suggesting its pathfinding role in episodic memory retrieval. *Learn. Mem.* **12**, 193–208 (2005).
25. Cheng, S. & Frank, L.M. New experiences enhance coordinated neural activity in the hippocampus. *Neuron* **57**, 303–313 (2008).
26. Tolman, E.C. Cognitive maps in rats and men. *Psychol. Rev.* **55**, 189–208 (1948).
27. Nader, K., Schafe, G.E. & LeDoux, J.E. The labile nature of consolidation theory. *Nat. Rev. Neurosci.* **1**, 216–219 (2000).
28. McKenzie, S. & Eichenbaum, H. Consolidation and reconsolidation: two lives of memories? *Neuron* **71**, 224–233 (2011).
29. Schoenenberger, P., O'Neill, J. & Csicsvari, J. Activity-dependent plasticity of hippocampal place maps. *Nat. Commun.* **7**, 11824 (2016).
30. Dupret, D., O'Neill, J., Pleydell-Bouverie, B. & Csicsvari, J. The reorganization and reactivation of hippocampal maps predict spatial memory performance. *Nat. Neurosci.* **13**, 995–1002 (2010).
31. Stark, E. *et al.* Pyramidal cell-interneuron interactions underlie hippocampal ripple oscillations. *Neuron* **83**, 467–480 (2014).
32. Mankin, E.A. *et al.* Neuronal code for extended time in the hippocampus. *Proc. Natl. Acad. Sci. USA* **109**, 19462–19467 (2012).
33. Woodworth, R. *Dynamic Psychology.* (Columbia University Press, 1918).
34. Vanderwolf, C.H. Hippocampal electrical activity and voluntary movement in the rat. *Electroencephalogr. Clin. Neurophysiol.* **26**, 407–418 (1969).
35. Muller, R.U., Stead, M. & Pach, J. The hippocampus as a cognitive graph. *J. Gen. Physiol.* **107**, 663–694 (1996).
36. Muller, R.U. & Kubie, J.L. The effects of changes in the environment on the spatial firing of hippocampal complex-spike cells. *J. Neurosci.* **7**, 1951–1968 (1987).
37. Ziv, Y. *et al.* Long-term dynamics of CA1 hippocampal place codes. *Nat. Neurosci.* **16**, 264–266 (2013).
38. Mehta, M.R., Barnes, C.A. & McNaughton, B.L. Experience-dependent, asymmetric expansion of hippocampal place fields. *Proc. Natl. Acad. Sci. USA* **94**, 8918–8921 (1997).
39. Monaco, J.D., Rao, G., Roth, E.D. & Knierim, J.J. Attentive scanning behavior drives one-trial potentiation of hippocampal place fields. *Nat. Neurosci.* **17**, 725–731 (2014).
40. Kentros, C.G., Agnihotri, N.T., Streater, S., Hawkins, R.D. & Kandel, E.R. Increased attention to spatial context increases both place field stability and spatial memory. *Neuron* **42**, 283–295 (2004).
41. Tse, D. *et al.* Schemas and memory consolidation. *Science* **316**, 76–82 (2007).
42. Lee, I., Yoganarasimha, D., Rao, G. & Knierim, J.J. Comparison of population coherence of place cells in hippocampal subfields CA1 and CA3. *Nature* **430**, 456–459 (2004).
43. Kemere, C., Carr, M.F., Karlsson, M.P. & Frank, L.M. Rapid and continuous modulation of hippocampal network state during exploration of new places. *PLoS One* **8**, e73114 (2013).
44. Stark, E., Roux, L., Eichler, R. & Buzsáki, G. Local generation of multineuronal spike sequences in the hippocampal CA1 region. *Proc. Natl. Acad. Sci. USA* **112**, 10521–10526 (2015).
45. Dupret, D., O'Neill, J. & Csicsvari, J. Dynamic reconfiguration of hippocampal interneuron circuits during spatial learning. *Neuron* **78**, 166–180 (2013).
46. Kamondi, A., Acsády, L. & Buzsáki, G. Dendritic spikes are enhanced by cooperative network activity in the intact hippocampus. *J. Neurosci.* **18**, 3919–3928 (1998).
47. Magee, J., Hoffman, D., Colbert, C. & Johnston, D. Electrical and calcium signaling in dendrites of hippocampal pyramidal neurons. *Annu. Rev. Physiol.* **60**, 327–346 (1998).
48. Golding, N.L., Staff, N.P. & Spruston, N. Dendritic spikes as a mechanism for cooperative long-term potentiation. *Nature* **418**, 326–331 (2002).
49. Bittner, K.C. *et al.* Conjunctive input processing drives feature selectivity in hippocampal CA1 neurons. *Nat. Neurosci.* **18**, 1133–1142 (2015).
50. Gomperts, S.N., Kloosterman, F. & Wilson, M.A. VTA neurons coordinate with the hippocampal reactivation of spatial experience. *eLife* **4**, e05360 (2015).

ONLINE METHODS

Subjects and electrode implantation. All experiments were approved by the Institutional Animal Care and Use Committee of New York University Medical Center. We used transgenic mice to obtain expression of exogenous light-sensitive opsins[51]: four mice expressed archaerhodopsin-3 (ref. 52) (Arch) under control of the pyramidal cell selective calcium/calmodulin-dependent protein kinase II alpha (CaMKIIα) promoter (referred to as CaMKII-cre::Arch) and one mouse expressed channelrhodopsin-2 (ref. 53) (ChR2) under the parvalbumin (PV) promoter, primarily expressed in a subpopulation of inhibitory interneurons (referred to as PV-cre::ChR2; **Supplementary Figs. 1** and **5** and **Supplementary Table 1**). The inclusion of the PV-cre::ChR2 mouse did not change the overall conclusions drawn from our study (**Supplementary Fig. 2**). Mice were obtained by breeding the Cre-dependent 'responder' lines expressing Arch (*Ai35D* allele; Jackson stock no. 012735) and ChR2 (*Ai32* allele; Jackson stock no. 024109) with the 'driver' lines expressing Cre recombinase under the CaMKIIα[54] (Jackson stock no. 005359) and PV[55] (Jackson stock no. 008069) promoters. These five adult male mice (3–5 months old) were implanted unilaterally or bilaterally with high-density silicon probes (32 or 64 sites; Buz32 or Buz64; NeuroNexus) attached to movable microdrives (**Fig. 1a**), under isoflurane anesthesia, as described previously[56]. In all experiments, ground and reference screws were implanted in the bone above the cerebellum. Probes were implanted perpendicularly to the midline, or with a 45° angle along the hippocampal long axis, at the following coordinates: AP: −1.7 mm; ML: +1 or −1 mm (left or right hemisphere). Two mice were implanted at AP: −1.8; ML: ±1.4. During surgery, the tips of the probes were lowered to the neocortex (depth: 700 μm). After 4–7 d of recovery, they were moved gradually (≤70 μm/day) until they reached the CA1 pyramidal cell layer of the dorsal hippocampus, characterized by large-amplitude ripple oscillations. Neuronal spiking activity and LFP were recorded daily in the behavioral task (**Fig. 1a**) and the position of the probe was optimized at the end of each daily session to obtain the maximal unit yield. The composition of the spiking population varied from session to session due to either active movement of the probe or to spontaneous movement of the brain tissue. We cannot exclude some overlap between the units recorded in the different sessions from the same animal. However, this was not considered to be an issue, since we varied the positions of the rewards on the maze from day to day (new learning), as well as other parameters such as the type of light stimulation (with or without delay) and the identity of the illuminated shanks (for mice with multiple diodes). At the end of the experiment, electrolytic lesions were created by passing current through the bottom sites of the shanks (5 μA for 5 s), and mice were killed for analysis 2 d later. Probe shank locations were verified by histology (**Supplementary Fig. 1b**,**c**).

Diode-probes. The probes consisted of 4 or 8 shanks (200-μm shank separation) and each shank had 8 recording sites (160 μm^2 per site, 1–3-MΩ impedance), staggered to provide a two-dimensional arrangement (20-μm vertical separation; Buz32 or Buz64; NeuroNexus). One or more multimode optical fibers (core diameter: 50 μm) were attached to the probe shanks, terminating in a tip etched to a point above electrode sites. At the other end, fibers were coupled to laser diodes[56] (450-nm blue laser diode for ChR2 activation; 639-nm red laser diode or 520-nm green laser diode for Arch activation; **Fig. 2a**). Both red and green illumination could effectively suppress pyramidal cell spiking in CaMKII-cre::Arch mice. Peak light power, measured at the tip of the shanks before implantation, was: 191 ± 11 μW (mean ± s.e.m.; n = 2 blue laser diodes), 320 ± 73 μW (n = 3 red laser diodes) and 151 ± 19 μW (n = 6 green laser diodes).

Data acquisition. During the recording session, neurophysiological signals were acquired continuously at 20 kHz on a 256-channel Amplipex system (Szeged, Hungary; 14-bit resolution, analog multiplexing)[57]. The wide-band signal was downsampled to 1.25 kHz and used as the LFP signal. A three-axis accelerometer (ADXL-330, Analog Devices) was attached to the signal multiplexing headstage for monitoring movements. To track the position of the mouse on the cheeseboard maze and in its home cage, two small LEDs, mounted above the headstage, were recorded by a digital video camera at 30 frames/s. The LED locations were detected and recorded online with custom-made tracking software.

Pretraining. All mice were free from prior manipulation before being included in this study and were maintained on a 12-h:12-h light:dark cycle (lights on at 7:00 a.m.) in the vivarium (maximum 5 adult mice per cage; housed individually after surgery). Before electrode implantation, the mice were handled daily for at least 1 week and pretrained on the spatial learning task on the cheeseboard maze. All experiments were done during the day (light cycle). Pretraining consisted first of simple exposure to the platform and the start box, for 1 h daily for 2 d, while water deprivation started. On the following 2 d, the mouse was allowed to collect ~20 water rewards (10 μL each) placed in the wells at random locations on the maze. On subsequent days, the animal was trained to locate three water rewards per trial (see below). No probe test was conducted during pretraining. Pretraining was completed when the mouse was able to perform at least 20 trials per session (3 to 4 d). The mouse was then allowed to recover from water deprivation and regain full weight.

Behavioral training. Mice were trained to perform a spatial learning task on a cheeseboard maze, similar to the task previously described for rats[30,58]. The maze consisted of a circular platform 80 cm in diameter with 177 wells (1.5 mm deep; 4 mm in diameter; 5 cm spacing between the wells) and a start box placed next to the platform (**Fig. 2d**). Access to the platform from the start box and to the start box from the platform was controlled by a manually operated door. Each daily session consisted of five epochs during which hippocampal activity and behavior were continuously recorded: (i) a prelearning exploration epoch, (ii) a rest epoch, (iii) a learning task, (iv) a rest epoch and (v) a postlearning exploration epoch (**Fig. 1a**). For the two rest epochs, the animal was returned to its home cage and allowed to sleep for ~1 h. During these rest epochs, the light in the recording room was on in order to favor sleep, whereas only dim light was used during the learning task and the pre- and postexploration epochs. The mouse was exposed to the cheeseboard maze during the two exploration epochs and the learning task. During the learning task, mice learned the locations of three hidden water rewards (5 μL) on the cheeseboard maze, out of 177 possible wells (**Fig. 1c**). A new set of three baited wells was randomly selected every day but stayed fixed within a given day. A trial was completed once the mouse had retrieved the three rewards and returned to the start box (median: 50 trials; range: 29–60 trials; n = 29 sessions, 5 mice). Access to the start box was conditioned upon successful retrieval of the three baits. However, a trial was aborted and the animal was allowed to return to the start box in the rare cases when the three water rewards were not collected within 4 min (from trial start). To prevent the possible use of an odor-guided search strategy that could interfere with spatial learning, the cheeseboard platform was rotated relative to the start box between trials. In addition, the maze was wiped after every five trials and at the end of each Pre and Post exploration epoch with a tissue soaked in alcohol. Thus, goal locations were defined in an extra-maze reference frame. The Pre and Post exploration epochs were used to (i) test memory performance and (ii) obtain the place fields of the recorded cells for the entire maze. Each epoch was divided into three periods (or 'blocks') of 10 min:

Block 1: free exploration without any reward;

Block 2: the mouse was presented with a first set of five water rewards placed at random locations (same locations for the Pre and Post explorations) to encourage exploration of the entire maze; and

Block 3: the mouse was presented with a second set of five water rewards placed at random locations (same locations for the Pre and Post explorations) to encourage exploration.

Blocks 2 and 3 were therefore identical (random search) but the rewards were replenished halfway through. The mouse was allowed to return to the start box between each block. This strategy was used to promote complete spatial exploration of the platform, a necessary condition for studying the spatial information coded by hippocampal assemblies. For quantifying memory performance after learning, only the first (unbaited) block of each pre- or postlearning exploration epoch was considered, whereas all three blocks were used for comparing place cell activity. Memory performance was assessed by calculating the proportion of time the mouse spent in the goal areas (15 cm diameter circular regions centered on goal locations) relative to the block duration (10 min) in the Pre and Post exploration epochs (**Fig. 1d**). When comparing learning performance in ripple-delayed and ripple-locked conditions, only sessions in which a single type of stimulation was delivered during learning were considered (i.e., we excluded sessions in which both ripple-locked and ripple-delayed stimulations were used in different hemispheres). Learning performance during the learning task was assessed by the distance traveled to retrieve the rewards during each trial or the time it took for the mouse to collect the three rewards (**Fig. 1c**).

In a subset of sessions (10 sessions in 4 mice), the learning task was modified and the locations of the rewards were signaled by white plastic cylinders, placed next to the baited wells ('cue-guided version' of the task)[30]. Under these conditions, the animal reached maximal performance during the first trial and, therefore, the learning curve was flat (**Supplementary Fig. 13a**). Optogenetic manipulations were conducted as described previously for the noncued version of the task.

Unit clustering and neuron classification. Spikes were extracted from the high-pass filtered signals (median filter, cutoff frequency: 800 Hz) offline. The waveforms were projected onto a common basis obtained by principal component analysis (PCA) of the data and sorted into single units automatically using KlustaKwik[59], followed by manual adjustment using the software Klusters[60] (http://neurosuite.sourceforge.net). For each unit, the single recording site with the maximal trough-amplitude mean waveform was selected and two waveform features were computed: the trough-to-peak and the spike width (the inverse peak frequency of the spike spectrum, estimated by 1,024-point FFT of the zero-padded waveforms). This generated two clearly separable clusters (**Supplementary Fig. 3a**). Putative pyramidal neurons (PYR) and interneurons (INT) were identified based on a Gaussian-mixture model using these two waveform features[61]. This model was previously built on the waveforms of optogenetically tagged neurons and neurons showing monosynaptic connections in the hippocampal CA1 region. It enabled assigning a P value to the classification of each unit, and units with low classification confidence ($P > 0.05$) were discarded (21/1,406 units, 1.5%). When the identity of a unit defined by this method was considered ambiguous, it was also excluded from the analysis (138/1,406 units, 9.8%). Classification of units as PYR and INT was done blindly, i.e., without a priori knowledge of the group the unit belonged to (Control, Delayed or Silenced). We recorded a total of 1,406 well-isolated units from CA1 of five freely moving mice in 29 sessions (**Supplementary Table 1**). Of these, 1,020 were putative pyramidal cells and 227 were putative interneurons. We could not classify 159 well-isolated units. The stability of our unit recordings across each daily session was checked by comparing the Mahalanobis distance (how well a given unit was isolated from other unit clusters) and the spike waveform amplitude (on the electrode site with maximal amplitude) in the pre- and postexploration epochs (**Supplementary Fig. 11a**–**d**).

Optogenetic suppression of pyramidal neurons. The response of each recorded unit to light was tested with a series of light pulses applied during the first rest epoch of each daily recording session (~300 pulses per LD, 100 ms each, one pulse every 5 s). This response-mapping procedure allowed us to compare the firing rate of each unit before (baseline) and during the light pulses (baseline: 100 ms intervals starting 1 s before each stimulus onset). A unit was considered light-suppressed when the mean firing rates during the light pulses (R_{light}) were significantly reduced as compared to baseline activity (R_{baseline}; $P < 0.05$, Wilcoxon's signed-rank test for matched values, one-tailed test). We computed the light-response index for each unit according to the following formula:

$$\text{Light-response index} = (R_{\mathrm{light}} - R_{\mathrm{baseline}})/(R_{\mathrm{light}} + R_{\mathrm{baseline}})$$

An index of value 0 indicates no change as compared to baseline; −1 indicates complete silencing (**Supplementary Figs. 3b** and **4**). For bilateral light delivery and recording, only the response to the light stimulus delivered ipsilaterally to the recorded cell was considered. Units classified as Control included nonsignificantly modulated neurons (neither suppressed nor excited during light pulses; $P > 0.05$, Wilcoxon's signed-rank tests) recorded exclusively from nonilluminated shanks (**Fig. 2f,g**). Of the 1,020 recorded putative pyramidal cells, 79 were excluded because they were not identified as light-responsive and were located on illuminated shanks (excluded Control cells) and 59 were excluded because they showed an increased activity during light pulses. A neuron was also discarded if its baseline firing rate was too low to determine whether a spike count of zero during light pulses was distinct from the spike count expected by chance (20 out of 1,020 pyramidal cells). Assuming a Poisson distribution of the neuron spike counts, the minimal (expected) number of spikes during the total light pulse duration (lambda) that could, simply by chance, result in 0 spikes is 3 for an alpha level of 0.05. Therefore, with 30 s of response-mapping light pulses (300 pulses of 100 ms), cells that fired less than 0.1 spikes/s during baseline were excluded. Of the remaining putative pyramidal cells, 273 units were silenced by SPW-R-triggered light pulses, 129 units were silenced with a delay (100–300 ms following SPW-R detection) and 460 served as Control units.

SPW-R-triggered closed-loop light stimulation. A single channel from the middle of the CA1 pyramidal cell layer with the largest amplitude ripple was selected for real-time processing of LFP by a programmable digital signal processor (DSP) running at 25 kHz (RX6, Tucker-Davis Technologies). The root-mean-square (RMS) of the bandpass-filtered (80–250-Hz) signal was computed in two running windows, long (2 s; RMS1) and short (8 ms; RMS2). Ripples were defined as events with RMS2 exceeding 3× RMS1 (range: 3–3.5) for at least 8 ms (ref. 31). Light stimuli (60-ms square pulses, 1 pulse per detection) were applied in a closed-loop manner during the learning task, exclusively when the mouse was located at the reward locations (15-cm diameter circular areas centered on the three baited wells; 'ripple-locked' condition; **Fig. 2d**). This spatially conditioned stimulation was achieved using custom tracking software, which detected, in real time, the periods when the mouse was located within the predefined goal areas. As a control, delayed stimuli (60-ms pulses, 1 pulse per detection) were presented at random intervals between 100 and 300 ms following SPW-R detection ('ripple-delayed' condition). Ripple-delayed and ripple-locked conditions were presented in a pseudorandomized manner in the same animal subjects, either on different recording sessions or in combination but in different hemispheres (**Supplementary Table 1**).

To quantify the effectiveness of the online SPW-R detection, we used the first 3 min of the postlearning epoch when the online detection was conducted but no light stimulus was delivered. During this period, the mouse was in the start box before being released for exploration. SPW-Rs that occurred during immobility periods (movement < 3cm/s) were visually identified in each session blindly (without the knowledge of online detection times) and subsequently compared to the online detections. Overall, 83 ± 4% of the visually identified SPW-Rs were detected by the online detection program ($n = 17$ sessions). The SPW-Rs missed by online detection were typically smaller amplitude events and shorter in duration as compared to online-detected SPW-Rs. Conversely, 63 ± 4% of all online detected SPW-Rs were considered false-positive events by visual scoring. These false-positive events were typically due to muscle artifacts or large-power fast gamma events during small movements. These falsely detected SPW-Rs necessitated the inclusion of delayed-stimulation control experiments.

Offline detection of SPW-Rs was performed as previously reported[31] to estimate awake SPW-Rs duration and the delay between online SPW-R detection and SPW-R onset (**Supplementary Fig. 6**; postexploration epoch or learning task epoch with Delayed conditions only) and to characterize changes in sleep SPW-Rs activity during slow-wave sleep (**Supplementary Fig. 14**). Briefly, the wide-band signal was bandpass-filtered (80–250 Hz; difference-of-Gaussians, DOG; zero-lag, linear phase FIR), and instantaneous power was computed. The mean and s.d. were computed from the power of the signal during slow-wave sleep in the absence of light stimulation. Subsequently, the power of the original trace was computed, and all events exceeding 2.5 s.d. from the mean were selected. Short events (duration < 15 ms) were discarded, and adjacent events (gap < 15 ms) were merged. Events were then expanded until the power fell below 2 s.d. to define event edges. Slow-wave sleep periods were defined using hippocampal LFP (theta/delta ratio) and accelerometer (movement) data, as previously described[62].

Spatial tuning of place cell activity. Data recorded on the cheeseboard maze were used for to analyze the spatial tuning of spiking activity. Only data recorded during epochs when the mouse was running faster than 5 cm/s were used. The position of the animal was determined by recording LEDs on the head stage at 30 Hz using custom-made tracking software. The position and spiking data were sorted into 3-cm × 3-cm bins to generate raw maps of spike counts and occupancy. A Gaussian kernel (s.d. = 5 cm) was applied for raw maps of both spike and occupancy, and a smoothed rate map was constructed by dividing the smoothed spike map by the smoothed occupancy map. The smoothed rate maps obtained for the prelearning and postlearning exploration epochs were used to compute the mean and peak firing rates in the maze as well as the number of place fields. A place field was defined as a contiguous region of at least 72 cm^2 (8 bins) in which the firing rate was above 60% of the peak rate in the maze, containing at least one bin above 80% of the peak rate in the maze[63]. Sparsity, spatial selectivity and spatial information[64] were computed from the smoothed rate maps[63,65]. Units with peak firing rates lower than 0.4 Hz and information content lower than 0.25 bits/spike were not considered as place cells. If the information content of the cell was similar ($P > 0.05$) to chance level (computed by parsing the spike train of the cell and mouse position (only when speed > 5 cm/s) into 30-s blocks and shuffling these 'spike' and 'position' blocks 100× relative to each other[65]), the cell was also not a considered a place cell. Only putative pyramidal cells that were defined as place cells in the cheeseboard maze (start box excluded) in at least one of the two exploration epochs (pre- or postlearning) were considered for the analyses. Of the 1,020 putative pyramidal cells, 637 were classified as place cells in the maze: 167 were silenced by SPW-R-triggered light pulses ('Silenced'), 81 were silenced with a delay after SPW-R detection ('Delayed') and 283 were control place cells ('Control'). Of the 106 remaining place cells, 15 were discarded because they had undefinable responses due to low firing rates, 52 were discarded because they were nonresponsive and located on illuminated shanks and 39 were discarded because they showed an increase in activity during the light pulses (see "Optogenetic suppression of pyramidal neurons," above).

Statistical analyses. All statistical analyses were performed in Matlab (MathWorks). The numbers of animals and recorded cells were similar to those generally employed in previous reports[12–14,25,29,30,38,39,66] (**Supplementary Table 1**). All tests were two-tailed unless otherwise indicated. For all tests, nonparametric Mann-Whitney *U* tests, Wilcoxon's paired signed-rank tests and Kruskal-Wallis one-way ANOVA were used. Tukey's *post hoc* tests were performed for multiple comparisons. Analysis of place cells' properties (remapping, place field characteristics) was done blindly relative to the cell categories these cells belonged to (approach 1: Control, Delayed and Silenced groups; or approach 2: ripple-locked or ripple-delayed groups). Outlier values not represented in **Figure 4** and **Supplementary Figure 8f**,**g** were included in statistical analyses (their exclusion does not affect the conclusions). Results are displayed as mean ± s.e.m. unless indicated otherwise. When box plots are used (for example, in **Fig. 2c**,**g**), on each box, the central mark indicates the median, and the bottom and top edges of the box indicate the 25th and 75th percentiles, respectively. The whiskers extend to the most extreme data points not considered outliers, and the outliers are plotted individually using the '+' symbol. A **Supplementary Methods Checklist** is available.

Quantification of spatial map stability. Place map stability for individual place cells was defined by the bin-by-bin Pearson's correlation coefficient between the firing rate maps of the Pre and Post exploration epochs. Only spatial bins visited by the mouse for at least 100 ms during both epochs were taken into account.

Place field overlap. Spatial bins of place fields were defined as described above. The percentage of overlap between pre- and postexploration place fields represents the area covered by the intersection between the Pre and Post place fields (**Supplementary Fig. 8a**,**c**) divided by the area covered by their sum. A place cell was considered to have non-overlapping place fields if it displayed Pre and Post place fields that had no spatial bins in common (**Supplementary Fig. 8b**). Place cells that had place fields in one probe session but no place fields in the other probe session were also considered as having non-overlapping place fields. Using less restrictive criteria for place field definition did not affect our observations (**Supplementary Fig. 8d**,**e**).

Population vector analysis. Among all recording sessions, we identified sessions with at least 5 place cells ('ensembles') in a given category (Silenced, Control or Delayed; range: 5 to 28 place cells). For each ensemble, we computed the correlation value obtained for individual spatial bins between the prelearning and postlearning exploration epochs[30,66]. The stability score corresponded to the median of these per-bin correlation values obtained for a given ensemble of place cells. Only bins visited by the animal for longer than 100 ms during both prelearning and postlearning exploration epochs were included in this analysis. For the comparison of pairs of simultaneously recorded ensembles (**Fig. 6**), we used a down-sampling approach in order to control for ensemble size. First, the number of place cells part of the smaller ensemble of the pair (*N*) was determined. Next, we randomly selected *N* cells from the larger ensemble of the pair and computed the corresponding stability score as previously described. We repeated this procedure up to 100 times and computed the average stability score obtained from the scores of down-sampled ensembles. This averaged stability score was assigned to the larger ensemble of the pair (**Supplementary Fig. 12**).

Goal location representation. *Probability of spiking in goal areas*. For each neuron, we first computed a 'probability map' that indicated the probability of the neuron to emit an action potential in a spatial bin of the maze per time unit. This map was obtained by dividing the rate map of the neuron by the sum of the rates accumulated over all visited spatial bins. From this probability map, we then added the probability values corresponding to the visited spatial bins surrounding the three goal locations (circular areas with 5-cm radii centered on the goal wells). The resulting value was then normalized by dividing it by the total number of spatial bins included in the sum. This procedure was done independently for the prelearning and postlearning exploration epochs (**Supplementary Fig. 15a**).

Distance of place field to goal areas. Place fields were defined as described previously. For each place field, the shortest distance between its (i) edge, (ii) peak or (iii) centroid and any of the three goal locations was determined. If a neuron had multiple place fields, only the minimal value was considered (i.e., the place field closest to any goal location) (**Supplementary Fig. 15b**).

Histological processing. Mice were anesthetized with pentobarbital (100 mg/kg intraperitoneal) and perfused with saline and 4% paraformaldehyde before their brains were rapidly removed. Coronal sections (100 μm) were cut on a vibratome (Leica, VT1000S) and collected in phosphate-buffered saline (PBS).

DAPI staining. After three washes in PBS (10 min each), sections were permeabilized in PBS containing 0.2% Triton-X100 (PBS*) for 20 min. Sections were then incubated for 20 min in PBS* containing DAPI (1:10,000; D1306, Molecular Probes) and washed again three times (10 min each) in PBS. Sections were mounted in Fluoromount (Sigma) and imaged with a wide-field fluorescence microscope (Zeiss, Axioscope).

Parvalbumin (PV) immunostaining. After three washes in PBS (10 min each), sections were permeabilized in PBS containing 1.5% goat serum and 0.2% Triton-X100 (PBS*) for 1 h and processed for immunostaining by overnight incubation at 4 °C with polyclonal antibodies anti-PV diluted in PBS* (1:500; PV 27, Swant, https://www.swant.com/pdfs/Rabbit_anti_parvalbumin_PV27.pdf). After two washes (30 min each) in PBS, sections were incubated for 2 h at room temperature (20–24 °C) with secondary antibodies (goat anti-rabbit IgGs conjugated with Alexa Fluor 555 dyes; 1:3,000; Molecular Probes) and DAPI (1:10,000). After three washes (20 min each), sections were mounted in Fluoromount (Sigma) and imaged with a confocal laser-scanning microscope (Zeiss, LSM 800).

Data availability. The data that support the main findings of this study will be publicly available on the CRCNS server (http://crcns.org/; estimated date of release: August 2017).

Code availability. Most of the code used was adapted from the FMAToolbox (http://fmatoolbox.sourceforge.net/). The code used in this study is available from the corresponding author upon request.

51. Madisen, L. *et al.* A toolbox of Cre-dependent optogenetic transgenic mice for light-induced activation and silencing. *Nat. Neurosci.* **15**, 793–802 (2012).
52. Chow, B.Y. *et al.* High-performance genetically targetable optical neural silencing by light-driven proton pumps. *Nature* **463**, 98–102 (2010).
53. Boyden, E.S., Zhang, F., Bamberg, E., Nagel, G. & Deisseroth, K. Millisecond-timescale, genetically targeted optical control of neural activity. *Nat. Neurosci.* **8**, 1263–1268 (2005).
54. Tsien, J.Z. *et al.* Subregion- and cell type-restricted gene knockout in mouse brain. *Cell* **87**, 1317–1326 (1996).
55. Hippenmeyer, S. *et al.* A developmental switch in the response of DRG neurons to ETS transcription factor signaling. *PLoS Biol.* **3**, e159 (2005).
56. Stark, E., Koos, T. & Buzsáki, G. Diode probes for spatiotemporal optical control of multiple neurons in freely moving animals. *J. Neurophysiol.* **108**, 349–363 (2012).
57. Berényi, A. *et al.* Large-scale, high-density (up to 512 channels) recording of local circuits in behaving animals. *J. Neurophysiol.* **111**, 1132–1149 (2014).
58. Kesner, R.P., Farnsworth, G. & Kametani, H. Role of parietal cortex and hippocampus in representing spatial information. *Cereb. Cortex* **1**, 367–373 (1991).
59. Harris, K.D., Henze, D.A., Csicsvari, J., Hirase, H. & Buzsáki, G. Accuracy of tetrode spike separation as determined by simultaneous intracellular and extracellular measurements. *J. Neurophysiol.* **84**, 401–414 (2000).
60. Hazan, L., Zugaro, M. & Buzsáki, G. Klusters, NeuroScope, NDManager: a free software suite for neurophysiological data processing and visualization. *J. Neurosci. Methods* **155**, 207–216 (2006).

 doi:10.1038/nn.4543

61. Stark, E. *et al.* Inhibition-induced theta resonance in cortical circuits. *Neuron* **80**, 1263–1276 (2013).
62. Grosmark, A.D., Mizuseki, K., Pastalkova, E., Diba, K. & Buzsáki, G. REM sleep reorganizes hippocampal excitability. *Neuron* **75**, 1001–1007 (2012).
63. Mizuseki, K., Royer, S., Diba, K. & Buzsáki, G. Activity dynamics and behavioral correlates of CA3 and CA1 hippocampal pyramidal neurons. *Hippocampus* **22**, 1659–1680 (2012).
64. Skaggs, W.E., McNaughton, B.L. & Gothard, K.M. in *Advances in Neural Information Processing Systems* Vol. 5 (Hanson, S.J., Cowan, J.D. & Giles, C.L., eds.) 1030–1037 (Morgan Kaufmann, 1993).
65. Markus, E.J., Barnes, C.A., McNaughton, B.L., Gladden, V.L. & Skaggs, W.E. Spatial information content and reliability of hippocampal CA1 neurons: effects of visual input. *Hippocampus* **4**, 410–421 (1994).
66. Leutgeb, J.K. *et al.* Progressive transformation of hippocampal neuronal representations in "morphed" environments. *Neuron* **48**, 345–358 (2005).